NANO LETTERS
Letter
pubs.acs.org/NanoLett

Dense Electron System from Gate-Controlled Surface Metal–Insulator Transition

Kai Liu,[†,‡,○] Deyi Fu,[†,§,○] Jinbo Cao,[†,‡] Joonki Suh,[†] Kevin X. Wang,[†] Chun Cheng,[†] D. Frank Ogletree,[∥] Hua Guo,[†,⊥] Shamashis Sengupta,[#] Asif Khan,[∇] Chun Wing Yeung,[∇] Sayeef Salahuddin,[∇] Mandar M. Deshmukh,[#] and Junqiao Wu*[,†,‡]

[†]Department of Materials Science and Engineering, University of California, Berkeley, California 94720, United States

[‡]Materials Sciences Division, Lawrence Berkeley National Laboratory, Berkeley, California 94720, United States

[§]School of Electronic Science and Engineering, Nanjing University, Nanjing, Jiangsu 210093, China

[∥]The Molecular Foundry, Lawrence Berkeley National Laboratory, Berkeley, California 94720, United States

[⊥]National Center for Electron Microscopy, Lawrence Berkeley National Laboratory, Berkeley, California 94720, United States

[#]Department of Condensed Matter Physics and Materials Science, Tata Institute of Fundamental Research, Homi Bhabha Road, Mumbai 400005, India

[∇]Department of Electrical Engineering and Computer Science, University of California, Berkeley, California 94720, United States

S *Supporting Information*

ABSTRACT: Two-dimensional electron systems offer enormous opportunities for science discoveries and technological innovations. Here we report a dense electron system on the surface of single-crystal vanadium dioxide nanobeam via electrolyte gating. The overall conductance of the nanobeam increases by nearly 100 times at a gate voltage of 3 V. A series of experiments were carried out which rule out electrochemical reaction, impurity doping, and oxygen vacancy diffusion as the dominant mechanism for the conductance modulation. A surface insulator-to-metal transition is electrostatically triggered, thereby collapsing the bandgap and unleashing an extremely high density of free electrons from the original valence band within a depth self-limited by the energetics of the system. The dense surface electron system can be reversibly tuned by the gating electric field, which provides direct evidence of the electron correlation driving mechanism of the phase transition in VO_2. It also offers a new material platform for implementing Mott transistor and novel sensors and investigating low-dimensional correlated electron behavior.

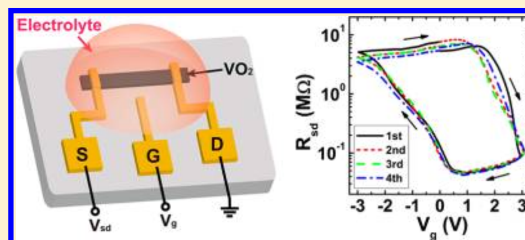

KEYWORDS: *Vanadium dioxide, 2D electron system, electrostatic gating, metal–insulator transition*

Electric-field tuning of surface carrier density is the fundamental mechanism of field-effect transistors and also attracts great attention as a method to control and explore new properties of electronic materials. Typically a high surface carrier density is realized via electrostatic gating, charge transfer, or electronic reconstruction in semiconductors and oxides.[1] Using electric-field tuning, conductive,[1,2] superconducting,[3−5] or magnetic[6] surface layers have been created on materials that originally do not possess these properties. However, the sheet carrier density achieved is typically below $\sim10^{14}$ cm^{-2} limited by factors such as breakdown field of the gate dielectric.[1,3] Higher densities are much desired in the exploration of correlated electron behavior in low dimensions.[7] In this regard, the possibility to induce and tune, by purely electrostatic means, a two-dimensional metallic layer on an insulating substrate is of great potential for reaching an ultrahigh surface carrier density. This could be realized by electric-field tuning of some phase transition materials, for example, vanadium dioxide (VO_2), which possesses a metal–insulator phase transition (MIT).

Vanadium dioxide exhibits a thermally driven MIT slightly above room temperature, while the role of electron correlation in the transition has been debated for decades.[8−11] Experiments show that the transition from the insulator phase to the metal phase is triggered when a threshold conductivity[12] or threshold free electron density[13] is reached by thermal excitation or compressive stress. However, the electron density threshold for the MIT is too high to be reached in charge accumulation by conventional solid gating.[14,15] As a result, experimental evidence of electrically activated MIT in VO_2 has been limited to those caused by current Joule heating[16] or Poole–Frenkel emission,[17] rather than electrostatic charge injection. Circumventing this limit, the electric double-layer transistor (EDLT) configuration uses an electrolyte or ionic liquid to produce an ultrahigh electric field on the order of 10^7 V/cm near the surface of the conduction channel,[18] driving electrostatic

Received: September 10, 2012
Revised: November 8, 2012
Published: November 19, 2012

 © 2012 American Chemical Society

accumulation of sheet charge density on the order of 10^{14} cm^{-2}. Very recently, gating of VO_2 thin films[19,20] and nanobeams[21] using liquid electrolyte have been reported. However, these groups attribute the large conductance modulation to two directly conflicting mechanisms, that is, electrochemically driven hydrogen doping[20] and electrostatically driven bulk MIT.[21] It is therefore necessary to elucidate the physics behind this intriguing effect. In this Letter, we show that the electrostatically accumulated surface charges trigger a surface metal–insulator transition (SMIT) on single-crystal VO_2 nanobeams and free up much higher density of electrons from the original valence band, resulting in a tunable and dense surface electron system on a substrate that has the same chemical composition as the electron layer.

VO_2 nanobeams were synthesized on silicon substrates with a 1.1-μm-thick thermal oxide layer using the vapor transport method reported previously.[22] Bulk VO_2 powder was placed in a quartz boat in the center of a tube furnace as the vapor source. The powder was heated at 1000 °C for 6 h with Ar as the carrier gas at a pressure of 10 Torr. VO_2 nanobeam products were collected on the substrates downstream from the powder. The first-order MIT of VO_2 occurs at 341 K with a drastic change of electrical conductivity and optical reflectivity between the insulator (I) phase and metal (M) phase. The I phase features a narrow bandgap separating the filled $d_{//}$ valence band and the empty π^* conduction band, and thermal activation of unintentional donors gives rise to a moderate density of free electrons; in the M phase, all electrons in the valence band are now turned into free electrons.[8] The free electron density increases from $\sim 10^{18}$ cm^{-3} in the I phase to $>10^{22}$ cm^{-3} in the M phase.[23] It was recently shown that single-crystal VO_2 nanobeams support single-domain MIT, which eliminates phase inhomogeneity and grain boundary effects typically existing in polycrystal thin films.[22,24] Figure 1 shows optical images of a VO_2 nanobeam device at 297 K (I phase, with bright contrast) and 393 K (M phase, with dark contrast), and its typical temperature-dependent resistance.

The electrolyte gating experiment is illustrated in Figure 1a. Cr/Au source, drain, and gate electrodes were defined via photolithography, deposited using e-beam evaporation, and annealed at 300 °C for 120 s to achieve ohmic contact. A comparison between four-probe and two-probe measurements showed that the contact resistance between source/drain electrodes and VO_2 was negligible. Using a needle probe, a droplet of electrolyte was applied onto the VO_2 nanobeam covering the entire conduction channel as well as the source, drain, and gate electrodes. The electrolyte is $KClO_4$ in 1000 MW polyethylene oxide (PEO) with a [K]:[O] ratio of 1:100.[3] Figure 1d shows the nanobeam resistance (R_{sd}) as a function of gate voltage (V_g) recorded at 318 K, at which temperature the electrolyte becomes a transparent liquid while the VO_2 channel is still in the I phase. In the measurement the source–drain current (I_{sd}) was recorded, while the source–drain voltage (V_{sd}) was kept at a constant low value (0.2–0.3 V) to avoid Joule heating. The leakage current between the gate and the source/drain (I_{leak}) electrodes was monitored and found to be always 1–3 orders of magnitude lower than I_{sd} for the entire range of V_g scanned (Figure S1). It can be seen that R_{sd} starts to decrease at $V_g \sim 1.5$ V and reaches a level nearly 2 orders of magnitude lower at $V_g = 3$ V. When V_g is scanned back, R_{sd} gradually recovers toward the original value but only after a wide hysteresis. This gate response is completely reversible: upon cyclic V_g sweeping, R_{sd} follows the same trace with nearly identical hysteresis. These effects were consistently observed from all devices (>15) measured, although the threshold gate voltage varies between 1 and 2 V from device to device. However, this hysteresis cannot be attributed to the kinetic behavior observed and expected from the low mobility of ions (see Supporting Information, Figure S2, S3, and the associated discussion). We note that I_{sd} vs V_{sd} is always linear at any given V_g, suggesting that the contacts are ohmic during the entire gating experiments (Figure S4).

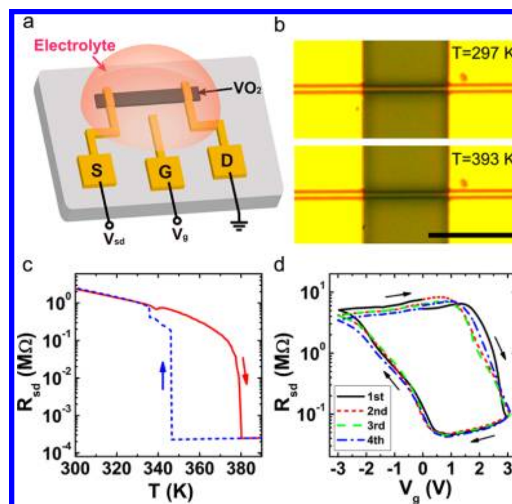

Figure 1. Electrolyte gating of single VO_2 nanobeams. (a) Schematic of the device configuration. (b) A VO_2 nanobeam below and above the MIT temperature (upper and lower panels, respectively). The scale bar is 10 μm. (c) A typical temperature-dependent source-drain resistance. (d) Source-drain resistance as a function of gate voltage for four sequential gate voltage scans. The scanning rate is 20 mV/s. The device has a rectangular cross section, with a size of about 10 μm in length, 600 nm in width, and 500 nm in thickness.

The high ON/OFF ratio in Figure 1d is not expected from conventional semiconductor behavior for the following reasons. In the I phase, the VO_2 nanobeam is a n-type semiconductor with unintentionally doped free carrier concentration between 10^{18} and 10^{19} cm^{-3}.[13,23,25] For such doped semiconductor channel with a thickness of 500 nm, we estimated that R_{sd} could be electrostatically modulated by no more than 3 times through surface free electrons accumulation. This can be easily understood in the following way: for a 500 nm thick semiconductor doped to 2×10^{18} cm^{-3}, the *sheet* charge density is 10^{14} cm^{-2}. As mentioned earlier, even with the ionic liquid gating, the maximum net sheet charge accumulation is on the order of 10^{14} cm^{-2} limited by the maximum V_g (to avoid dielectric breakdown or gate leakage). Therefore, the increase in total channel conductance is expected to be limited by a factor of a few (assuming no drastic change in mobility, which is the case of VO_2[23]). This is clearly due to the fact that the total channel conductance is dominated by the thick, moderately doped body, while the gate field can only accumulate a *limited* sheet density of free electrons near the surface. This is in stark contrast to thin film transistors that electrostatically achieve high ON/OFF ratios because of either a lightly doped (such as 10^{12} cm^{-3} in ref 26 and 10^{14} cm^{-3} in ref 27) or a ultrathin channel (such as 70 nm in ref 26 and 30 nm in ref 27), where the subsurface body conduction is negligible. It is estimated that, to achieve an ON/OFF ratio of ~ 100 by mere electrostatic charge accumulation in VO_2, either a background doping lower than 10^{16} cm^{-3} or a channel

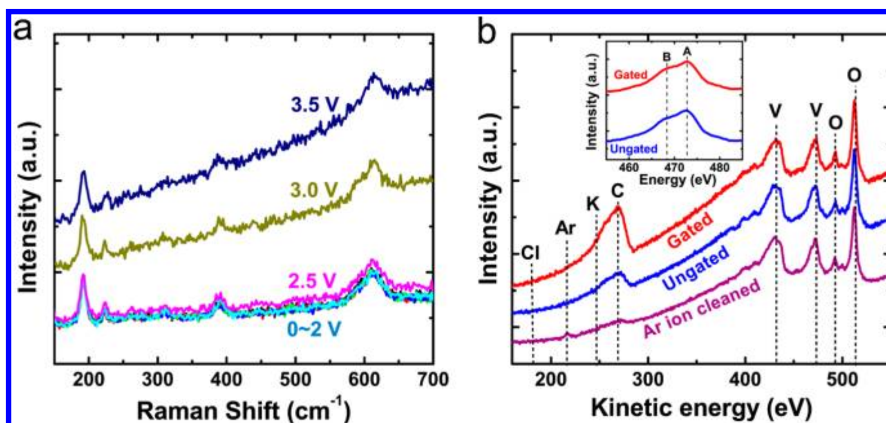

Figure 2. Raman and Auger characterization of VO_2 nanobeams. (a) Raman spectra at different gating voltages. (b) Nano Auger spectra for gated and ungated nanobeams, as well as a gated one with its surface cleaned by Ar ions in which the surface was removed by ∼1 nm.

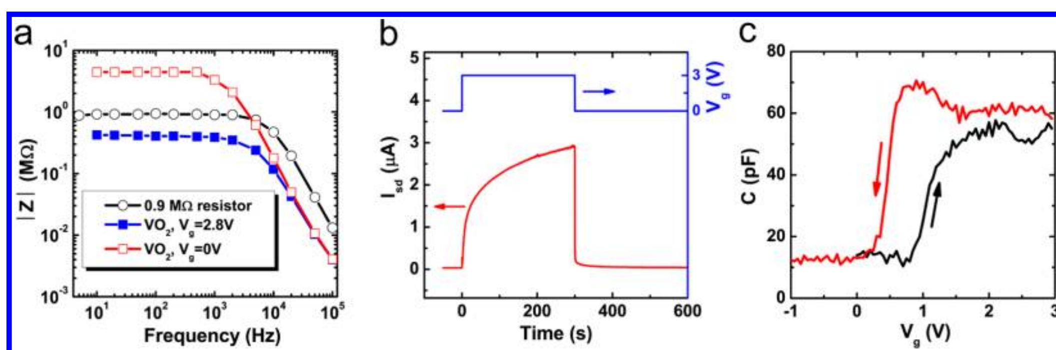

Figure 3. Temporal analysis of the gate response. (a) Frequency dependence of the source−drain impedance of a VO_2 nanobeam. The impedance of a 0.9 MΩ resistor is also shown for comparison. (b) Response of source−drain current to gate voltage change. Source−drain bias is fixed at 0.3 V. The VO_2 nanobeam used here is the same as that used in Figure 1d. (c) Capacitance of a VO_2 nanobeam as a function of gate voltage.

thickness thinner than 10 nm is needed, while our VO_2 specimens are unintentionally doped to $>10^{18}$ cm^{-3} and have a thickness of around 500 nm. To confirm this, a detailed numerical modeling using standard TCAD software is shown in the Supporting Information (Figures S5 and S6).

The key issues here are, whether this large modulation is dominated by electrostatically driven electronic phase transition, or electrochemically driven impurity doping, and whether it occurs on the surface or in the bulk. Nakano et al. suggest delocalized bulk MIT driven by electrostatic surface charge accumulation,[21] while Ji et al. propose electrochemical hydrogen doping.[20] To test these possible mechanisms, a series of analytical and electrical measurements were carried out. Figure 2a shows in situ Raman spectra taken on the gated VO_2 beam with V_g increasing from 0 to 3.5 V. The transparency of the electrolyte makes possible this type of in situ experiments. All of the Raman peaks resolved at ∼192 cm^{-1}, 223 cm^{-1}, 388 cm^{-1}, and 614 cm^{-1} are attributed to the I phase of VO_2 and are clearly unchanged in both intensity and position at different gate voltages. As the probe depth of the Raman reaches tens to hundreds of nanometers, this suggests that the bulk of the VO_2 is still in the I phase. Therefore, regardless of the conductance modulation effect being electrostatic or electrochemical, it must occur only on the surface of the VO_2, while the bulk of the VO_2 stay unmodulated. We note that the rise of the Raman background at high gate voltages (>2.5 V) in Figure 2a arises purely from the electrolyte, because a similar change was also observed from the electrolyte alone (Figure S7).

To further test the existence of possible electrochemical reactions or doping, nano Auger spectroscopy was utilized to characterize the surface composition of VO_2 with a detection depth <2 nm and spot size ∼10 nm, because Auger is known to be extremely surface sensitive to chemical composition. Two devices were made from the same VO_2 nanobeam and were both covered with the electrolyte, but only one device was gated at V_g = 2.8 V for 15 min. The electrolyte was washed away immediately after the gating, and both the gated and the ungated devices were probed by the nano Auger for comparison analysis. As clearly shown in Figure 2b, no Cl (LVV ∼ 181 eV) and K ($LM_{23}M_{23}$ ∼ 250 eV) signals were observed from the gated nanobeam, suggesting that the Cl^- and K^+ ions in the electrolyte did not diffuse and dope the VO_2 surface. Note that the wide carbon peak (∼270 eV) probably came from the residue of the electrolyte solvent, PEO. After Ar ion cleaning of the VO_2 surface, this carbon contamination was dramatically reduced (see Figure 2b). For the V $L_{23}M_{23}M_{45}$ line (∼470 eV), the two peaks (A and B, inset of Figure 2b) can be used to evaluate the valence of vanadium ions. The intensity ratio of peak A to B was reported to increase in going from V_2O_5 to VO_2 to V_2O_3 to V.[28] The ratio observed here, however, shows no difference for the gated and ungated nanobeams (inset of Figure 2b), which indicates that the valence of vanadium in the VO_2 surface is unaffected by the gating. Since electrochemical reactions are typically redox process, this observation suggests that surface electrochemical reactions are negligible in our electrolyte gating experiments.

dx.doi.org/10.1021/nl303379t | Nano Lett. 2012, 12, 6272−6277

Related to these analyses, a basic question is whether the channel conductance under gating is carried by electrons or ions. Figure 3a shows the amplitude of source–drain impedance ($|Z_{sd}|$) of a device measured for a range of frequencies using a lock-in amplifier. Under both zero and high gating voltages, $|Z_{sd}|$ remains independent of the driving frequency (f) for $f < \sim 10^3$ Hz. This indicates that the source–drain conduction of the VO_2 nanobeam at a gate voltage is carried by fast electronic motion, rather than ionic motion. For ionic motion limited transport, the impedance is expected to increase, as opposed to decrease, at frequencies that are too high for the ions to follow. The ultimate drop in $|Z_{sd}|$ in Figure 3a is attributed to an instrumental RC frequency cutoff, as shown by the measured impedance of a 0.9 MΩ resistor.

To further exclude the possibility that the specific chemistry of the electrolyte ($PEO/KClO_4$) plays a role in the conductance modulation of VO_2, we used another type of common ionic liquid, DEME-TFSI, to perform the same gating experiment. Before the measurement, the ionic liquid was carefully dried in vacuum ($\sim 10^{-5}$ Torr) at 110 °C for 15 h, and the devices we used were also dried under the same condition. A similar gate modulation of the channel resistance was still observed, together with a negligible leakage current through the gating medium (see Figure S8 in the Supporting Information). This indicates that the large conductance modulation is intrinsic to the material itself, as opposed to be due to specific chemistry of the chosen electrolyte.

Although we have excluded electrochemical reactions and K or Cl doping as the driving mechanism, the possibility of electrochemical protonation,[29] or hydrogen diffusion-in[20] as proposed recently has yet to be considered. It has been reported that the protonation of ZnO surface at a positive gate voltage in ionic liquid causes a large and hysteretic conductance modulation.[29] This is a chemisorption process with a large O–H bonding energy of 4.77 eV, and therefore the conductance modulation is shown to be nonvolatile; namely, the conductance stays at the gated value even if the gate voltage sweeps back to 0. The "erase" of the gating effect needs the gate voltage to be swept to a negative value exceeding a threshold. With VO_2 nanobeams, similar hydrogen doping mechanism was proposed to explain the hysteretic gate response in water-contained ionic liquid.[20] In this regard, a temporal study of the gate response would help to elucidate the possibility of protonation or hydrogen doping. Figure 3b shows a typical $I_{sd}(V_g)$ curve at fixed V_{sd} (= 0.3 V) while V_g was switched between 0 and 3 V. It can be seen that the gate response in our case is clearly *volatile*, which is inconsistent with a hydrogen diffusion-in process. When the V_g is switched on, a voltage drop (hence electric field) is established immediately between the VO_2 channel and the gate electrode, segregating ions in the liquid electrolyte toward the interface to establish the double layer. The relatively slow increase of I_{sd} is thus due to the low mobility of ions which have to move over a large distance (from the bulk of the electrolyte to the electrolyte-VO_2 interface). The removal of V_g rapidly suppresses I_{sd} over a short time, because these ions only need to diffuse away from the interface by a small distance to destroy the double layer, and consequently, I_{sd} quickly recovers to its original value (Figure 3b). In the picture of hydrogen diffusion-in, instead, the "erase" process upon the removal of V_g would be nonvolatile, or as slow as the "write" process upon the adding of V_g, similar in principle to the oxygen vacancy diffusion process.[3] Furthermore, we found that, after gating followed immediately by washing away the electrolyte, the channel resistance and I–V characteristics are totally unaffected. Combining this evidence, we conclude that the conductance modulation originates primarily from an electronic surface transition driven by electrostatics.

We emphasize that, although the change of the nanobeam resistance is as high as 3–4 orders of magnitude in the thermally induced bulk MIT, it is only 2 orders of magnitude by electrolyte gating. Together with the in situ Raman spectrum which shows definitively that the bulk of the gated VO_2 nanobeam is still in the I phase, this shows that the MIT occurs only in the surface layer. Nakano et al. proposed a MIT throughout the bulk of epitaxial VO_2 films with thicknesses less than 70 nm, for which the film is under high epitaxial strain from the substrate. In our case, however, single-crystal, strain-relaxed VO_2 nanobeams with thickness of 500 nm or more are used, and the MIT was seen to be limited to the surface. The difference in the depth of gated MIT may be attributed to the different thicknesses, strain states, and mechanical boundary conditions in these two types of samples.

Because the M and I phases of VO_2 support different electrodynamics, a capacitance–voltage (C–V) measurement would directly probe the SMIT. In these experiments, merely part of a VO_2 nanobeam ($\sim$200 μm in length and $\sim$1 μm in width) and the gate electrode ($\sim$200 μm in length and $\sim$200 μm in width) were covered by electrolyte. The differential capacitance between the gate electrode and VO_2 was recorded as a function of V_g. Because the capacitance of EDL near gate electrode is in series with and much larger than the VO_2/electrolyte capacitance, the measured differential capacitance is dominated by the EDL at the VO_2/electrolyte interface. A typical C–V curve is shown in Figure 3c. At the V_g threshold, C switches to a level 5 times higher. Before the SMIT, the total capacitance of the system is that of the electric double (Helmholtz) layer with a thickness $d_H \sim 1$ nm[3] in series with that of the VO_2 surface accumulation layer with a thickness on the order of the Debye–Hückel screening length $\lambda_{DH} = (\varepsilon k_B T/e^2 n)^{1/2} \sim 5$ nm.[30] Upon the SMIT, C is increased because the surface M layer strongly screens the VO_2 underneath, with only the Helmholtz layer capacitance alone left. Note that despite the extremely high *total* density of free electrons in the surface M layer of VO_2, the *net* electron density there is still relatively low, defined by the capacitance of and voltage drop across the Helmholtz layer. This is because the high density of additional free electrons was locally liberated from the VO_2 valence band, instead of externally injected from electrodes.

To understand the electronic process in which the surface of the VO_2 undergoes the SMIT at high V_g, we consider the energetics of the system including the electrolyte and the VO_2. Under a given V_g, we estimate the total energies of two scenarios; that is, the surface layer of the VO_2 remains in the I phase (A) or switches to the M phase (B). It is found that Scenario B becomes energetically more favorable than A as V_g is increased to a threshold V_{gth}, hence theoretically confirming the SMIT.

Figure 4a shows schematically the Scenario A (without SMIT) under V_g, in which electrons accumulate in the surface layer of VO_2 and screen the rest from the electric field. The total energy of the system (E^A_{total}) is composed of: (1) Gibbs free energy of VO_2 (G_I), (2) electrostatic energy stored inside the VO_2 accumulation layer ($E^A_{VO_2}$), and (3) electrostatic energy inside the Helmholtz layer (E^A_{HL}). In Scenario B (with SMIT)

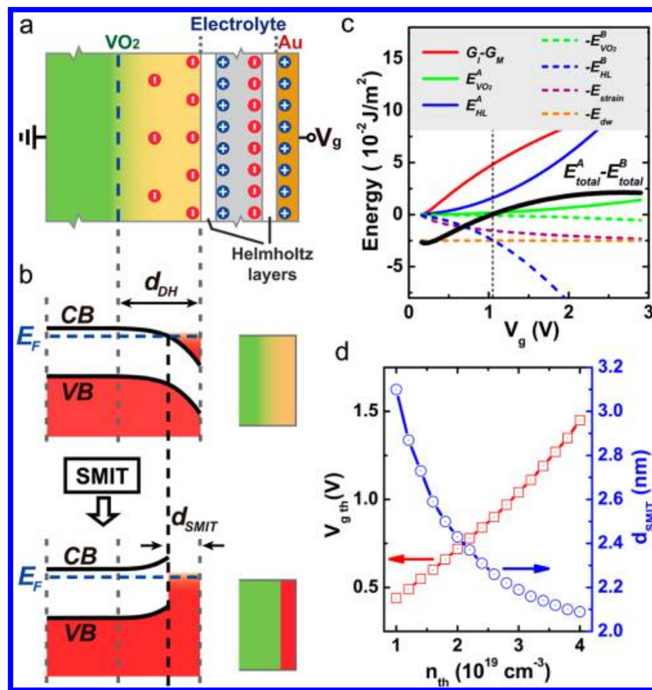

Figure 4. Energetics of the VO_2/electrolyte system. (a) Schematic of the electrolyte-gating system with an accumulation of electrons on the surface of VO_2. (b) Band diagrams of VO_2 without (upper) and with (lower) the SMIT. The surface charge density distribution is schematically shown to the right. (c) Calculated energy terms without the SMIT (solid curves) and with the SMIT (dashed curves) and the total energy difference (thick solid curve). The vertical dashed line indicates the threshold gate voltage for the total energy difference to change sign. (d) Calculated dependence of the threshold gate voltage and SMIT thickness as a function of the threshold carrier density required to trigger a MIT.

under the same V_g (Figure 4b), the difference is that the surface of VO_2 within a depth of d_{SMIT} becomes the M phase, where d_{SMIT} is the thickness of VO_2 in which the electron accumulation exceeds a threshold n_{th}. The total energy (E^{B}_{total}) is now: (1) M-phase Gibbs free energy (G_M), (2) electrostatic energy inside the VO_2 in both the M layer and the Schottky depletion layer immediately below ($E^{B}_{VO_2}$), (3) electrostatic energy inside the Helmholtz layer (E^{B}_{HL}), (4) energy of a domain wall separating the surface M layer and the VO_2 bulk I phase (E_{dw}), and (5) elastic energy stored throughout the thickness of d_{SMIT} because of misfit strain between the M and the I phases (E_{strain}).

Considering the high electron densities in the M phase (Scenario B), the Thomas–Fermi approximation was used to calculate the carrier distribution in depth, $n(z)$, with a screening length given by $\lambda_{TF} = (\varepsilon\pi^2\hbar^2/m^*e^2k_F)^{1/2}$, where $k_F = (3\pi^2 n)^{1/3}$ is the Fermi wavevector.[14] For I-phase VO_2 with nondegenerate carrier densities, the Debye–Hückel approximation was used with a screening length of λ_{DH}. All parameters were obtained from the literature, such as the effective mass ($m^* \sim 30m_0$ for the I phase and $5m_0$ for the M phase),[31] the dielectric constant ($\varepsilon \sim 24\varepsilon_0$ for the I phase[32] and $9\varepsilon_0$ for the M phase[33]), the contact potential between the M and the I phase ($\sim$ 0.3 eV), the domain wall energy density ($E_{dw} \sim 25$ mJ/m^2),[22] the M–I misfit strain (~0.01),[34] and the VO_2 elastic modulus (140 GPa).[35] When the carrier density n exceeds the threshold n_{th}, the M phase is thermodynamically favored, and G_M becomes lower than G_I. Their difference $\Delta G = G_I - G_M$ as a function of n can be estimated from the following $d\Delta G/dT = -\Delta S = -L/T$, where ΔS is the entropy change and L (~5 kJ/mol)[24] is the latent heat of the phase transition. Considering thermal activation of free electron density, $n \propto \exp(-E_a/k_BT)$, where $E_a \sim 0.36$ eV is the activation energy in I-phase VO_2,[13] we have $d \ln n/dT = -E_a/k_BT^2$. Consequently,

$$\Delta G(n) \approx \ln(n/n_{th})\cdot(d\Delta G/d \ln n) = \ln(n/n_{th})\cdot(L\cdot k_BT/E_a) \quad (1)$$

The overall change in ΔG was obtained by integrating $\Delta G(n)$ over the depth z using the solved $n(z)$ at different V_g. These energies were plotted in Figure 4c assuming $n_{th} = 3 \times 10^{19}$ cm^{-3} (see Supporting Information for calculation details). It can be seen that as V_g increases, $E^{A}_{total} - E^{B}_{total}$ switches sign at a threshold V_{gth}, and the surface of the VO_2 undergoes the SMIT.

The threshold electron density that triggers the SMIT, n_{th}, is unknown. The Mott criterion gives $n_{th} = 0.25/a_B \sim 10^{19}$ cm^{-3}, where a_B is the Bohr radius of electrons in the I phase.[14] Experimental evidence suggested $n_{th} \sim 8 \times 10^{18}$ cm^{-3}.[13] Figure 4d shows that, with n_{th} increasing from 1 to 4×10^{19} cm^{-3}, V_{gth} increases from 0.44 to 1.45 V. Over this range of parameters, however, the corresponding SMIT thickness (d_{SMIT}) remains 2–3 nm. We emphasize that, as the SMIT collapses the bandgap inside the surface M layer, free electrons with bulk density of 10^{22}–10^{23} cm^{-3} are liberated from the original valence band. Given the thickness of 2–3 nm, the sheet density of this electron system is estimated to be 10^{15}–10^{16} cm^{-2}. This is *much higher* than the maximum sheet density accumulated in electrostatically gated or modulation doped semiconductors and is also *an order of magnitude higher* than those typically achievable in complex oxide heterostructures.[1,3,7] Considering the strongly localized and correlated nature of the *d*-band that hosts the conducting electrons in the M state, here a truly two-dimensional electron liquid,[7] as opposed to electron gas, is electrostatically triggered and controlled on a substrate that has the same chemical composition as the active electron layer. Assuming an electron mobility of ~0.5 cm^2/(V s) for both the I and the M phases and $n \sim 10^{18}$ cm^{-3} and 10^{22} cm^{-3} for the I and M phases, respectively, the total resistance is estimated to be reduced due to the SMIT by 88–220 times for a VO_2 wire with radius ranging from 500 to 200 nm. This resistance reduction is consistent with the observed ON/OFF ratio of 80–100 in Figure 1d for a VO_2 nanobeam with a width/thickness of ~500 nm.

It should be noted that, once the surface M layer forms, it will completely screen the gating field and prevent expansion of the M layer along the VO_2 depth, so that d_{SMIT} is self-limited to $<$ ~3 nm, and R_{sd} remains at the same level even if V_g is further increased. The exact microscopic process of triggering the MIT when the n_{th} is approached is unclear; this calls for ab initio computation of this strongly correlated electron system at varying free electron density. The ultradense surface electron system can be reversibly tuned by the gating electric field, which provides direct evidence of the electron correlation driving mechanism of the phase transition in VO_2. It also offers a new material platform for implementing Mott transistor and novel sensors, and investigating low-dimensional correlated electron behavior.

dx.doi.org/10.1021/nl303379t | Nano Lett. 2012, 12, 6272–6277

■ ASSOCIATED CONTENT

Supporting Information

Measurements of electrolyte leakage current and source−drain resistance under various gate voltage sweeping modes, discussion of hysteresis and memory behavior, dependence of source−drain current on source−drain voltage at different gate voltages, numerical modeling of electrostatic field induced charge accumulation in VO_2, Raman spectra of electrolyte at various gate voltages, gating by using a different ionic liquid (DEME-TFSI), and details of energy calculation. This material is available free of charge via the Internet at http://pubs.acs.org.

■ AUTHOR INFORMATION

Corresponding Author

*E-mail: wuj@berkeley.edu.

Author Contributions

○These authors contributed equally.

Notes

The authors declare no competing financial interest.

■ ACKNOWLEDGMENTS

This work was supported by a NSF CAREER Award under the Grant No. DMR-1055938. The materials synthesis part was supported by the Director, Office of Science, Office of Basic Energy Sciences, Materials Sciences and Engineering Division, of the U.S. Department of Energy under Contract No. DE-AC02-05CH11231. The ionic liquid gating was partially supported by a seed grant from the NSF Center for Energy Efficient Electronics Science (NSF Award ECCS-0939514). We thank Ms. Allison Engstrom, Mr. Bryan W. Boudouris, and Dr. Hongtao Yuan for helpful discussions and Dr. Sefaattin Tongay and Dr. Michael Martin for technical assistance.

■ REFERENCES

(1) Ahn, C. H.; Triscone, J.-M.; Mannhart, J. *Nature* **2003**, *424*, 1015−1018.

(2) Scherwitzl, R.; Zubko, P.; Lezama, I. G.; Ono, S.; Morpurgo, A. F.; Catalan, G.; Triscone, J.-M. *Adv. Mater.* **2010**, *22*, 5517−5520.

(3) Ueno, K.; Nakamura, S.; Shimotani, H.; Ohtomo, A.; Kimura, N.; Nojima, T.; Aoki, H.; Iwasa, Y.; Kawasaki, M. *Nat. Mater.* **2008**, *7*, 855−858.

(4) Ye, J. T.; Inoue, S.; Kobayashi, K.; Kasahara, Y.; Yuan, H. T.; Shimotani, H.; Iwasa, Y. *Nat. Mater.* **2010**, *9*, 125−128.

(5) Ueno, K.; Nakamura, S.; Shimotani, H.; Yuan, H. T.; Kimura, N.; Nojima, T.; Aoki, H.; Iwasa, Y.; Kawasaki, M. *Nat. Nanotechnol.* **2011**, *6*, 408−412.

(6) Ohno, H.; Chiba, D.; Matsukura, F.; Omiya, T.; Abe, E.; Dietl, T.; Ohno, Y.; Ohtani, K. *Nature* **2000**, *408*, 944−946.

(7) Mannhart, J.; Schlom, D. G. *Science* **2010**, *327*, 1607−1611.

(8) Eyert, V. *Ann. Phys. (Leipzig)* **2002**, *11*, 650−702.

(9) Eyert, V. *Phys. Rev. Lett.* **2011**, *107*, 016401.

(10) Wentzcovitch, R. M.; Schultz, W. W.; Allen, P. B. *Phys. Rev. Lett.* **1994**, *72*, 3389−3392.

(11) Biermann, S.; Poteryaev, A.; Lichtenstein, A. I.; Georges, A. *Phys. Rev. Lett.* **2005**, *94*, 026404.

(12) Wei, J.; Wang, Z.; Chen, W.; Cobden, D. H. *Nat. Nanotechnol.* **2009**, *4*, 420−424.

(13) Cao, J.; Fan, W.; Chen, K.; Tamura, N.; Kunz, M.; Eyert, V.; Wu, J. *Phys. Rev. B* **2010**, *82*, 241101(R).

(14) Hormoz, S.; Ramanathan, S. *Solid-State Electron.* **2010**, *54*, 654−659.

(15) Sengupta, S.; Wang, K.; Liu, K.; Bhat, A. K.; Dhara, S.; Wu, J.; Deshmukh, M. M. *Appl. Phys. Lett.* **2011**, *99*, 062114.

(16) Gu, Q.; Falk, A.; Wu, J.; Ouyang, L.; Park, H. *Nano Lett.* **2007**, *7*, 363−366.

(17) Ko, C.; Ramanathan, S. *Appl. Phys. Lett.* **2008**, *93*, 252101.

(18) Prassides, K. *Nat. Nanotechnol.* **2011**, *6*, 400−401.

(19) Yang, Z.; Zhou, Y.; Ramanathan, S. *J. Appl. Phys.* **2012**, *111*, 014506.

(20) Ji, H.; Wei, J.; Natelson, D. *Nano Lett.* **2012**, *12*, 2988−2992.

(21) Nakano, M.; Shibuya, K.; Okuyama, D.; Hatano, T.; Ono, S.; Kawasaki, M.; Iwasa, Y.; Tokura, Y. *Nature* **2012**, *487*, 459−462.

(22) Wu, J.; Gu, Q.; Guiton, B. S.; de Leon, N. P.; Ouyang, L.; Park, H. *Nano Lett.* **2006**, *6*, 2313−2317.

(23) Ruzmetov, D.; Heiman, D.; Claflin, B. B.; Narayanamurti, V.; Ramanathan, S. *Phys. Rev. B* **2009**, *79*, 153107.

(24) Cao, J.; Ertekin, E.; Srinivasan, V.; Fan, W.; Huang, S.; Zheng, H.; Yim, J. W. L.; Khanal, D. R.; Ogletree, D. F.; Grossman, J. C.; Wu, J. *Nat. Nanotechnol.* **2009**, *4*, 732−737.

(25) Berglund, C. N.; Guggenheim, H. J. *Phys. Rev.* **1969**, *185*, 1022−1033.

(26) Chua, L.-L.; Zaumseil, J.; Chang, J.-F.; Ou, E. C.-W.; Ho, P. K.-H.; Sirringhaus, H.; Friend, R. H. *Nature* **2005**, *434*, 194−199.

(27) Nomura, K.; Ohta, H.; Takagi, A.; Kamiya, T.; Hirano, M.; Hosono, H. *Nature* **2004**, *432*, 488−492.

(28) Sawatzky, G. A.; Post, D. *Phys. Rev. B* **1979**, *20*, 1546−1555.

(29) Yuan, H.; Shimotani, H.; Tsukazaki, A.; Ohtomo, A.; Kawasaki, M.; Iwasa, Y. *J. Am. Chem. Soc.* **2010**, *132*, 6672−6678.

(30) Yim, J. W. L.; Jones, R. E.; Yu, K. M.; Ager, J. W., III; Walukiewicz, W.; Schaff, W. J.; Wu, J. *Phys. Rev. B* **2007**, *76*, 041303(R).

(31) *Collaboration: Authors and editors of the volumes III/17G-41D: VO2: resistivity, conductivity, photoconductivity*; Madelung, O., Rössler, U., Schulz, M., Eds.; Springer Materials - The Landolt-Börnstein Database (http://www.springermaterials.com), 2012, DOI: 10.1007/10681735_334.

(32) Kwan, C. C. Y.; Griffith, C. H.; Eastwood, H. K. *Appl. Phys. Lett.* **1972**, *20*, 93−95.

(33) Barker, A. S., Jr.; Verleur, H. W.; Guggenheim, H. J. *Phys. Rev. Lett.* **1966**, *17*, 1286−1289.

(34) Marezio, M.; McWhan, D. B.; Remeika, J. P.; Dernier, P. D. *Phys. Rev. B* **1972**, *5*, 2541−2551.

(35) Tsai, K.-Y.; Chin, T.-S.; Shieh, H.-P. D. *Jpn. J. Appl. Phys., Part 1* **2004**, *43*, 6268−6273.

Supporting Information for

Dense Electron System from Gate-Controlled Surface Metal-Insulator Transition

Kai Liu[1,2,‡], *Deyi Fu*[1,3,‡], *Jinbo Cao*[1,2], *Joonki Suh*[1], *Kevin X. Wang*[1], *Chun Cheng*[1], *D. Frank Ogletree*[4], *Hua Guo*[1,5], *Shamashis Sengupta*[6], *Asif Khan*[7], *Chun Wing Yeung*[7], *,Sayeef Salahuddin*[7], *Mandar M. Deshmukh*[6], *Junqiao Wu*[1,2,*]

[1] Department of Materials Science and Engineering, University of California, Berkeley, California 94720, USA

[2] Materials Sciences Division, Lawrence Berkeley National Laboratory, Berkeley, California 94720, USA

[3] School of Electronic Science and Engineering, Nanjing University, Nanjing, Jiangsu 210093, China

[4] The Molecular Foundry, Lawrence Berkeley National Laboratory, Berkeley, California 94720, USA

[5] National Center for Electron Microscopy, Lawrence Berkeley National Laboratory, Berkeley, California 94720, USA

[6] Department of Condensed Matter Physics and Materials Science, Tata Institute of Fundamental Research, Homi Bhabha Road, Mumbai 400005, India

[7] Department of Electrical Engineering and Computer Science, University of California, Berkeley, California 94720, USA

[‡] These authors contributed equally.

[*] To whom correspondence should be addressed. E-mail: wuj@berkeley.edu

1. Electrolyte leakage current.

The leakage current through the electrolyte I_{leak} is always 1~3 orders of magnitude lower than I_{sd} for the entire range of V_g scanned at the applied V_{sd} (0.2 V) as shown in Fig. S1. This rules out joule heating as the mechanism responsible for the observed large reduction in R_{sd}.

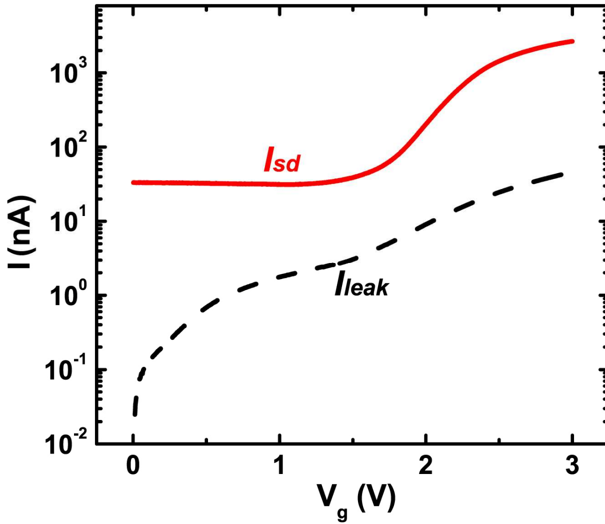

Figure S1. I_{sd}-V_g and I_{leak}-V_g curves. The V_g scanning rate is 20 mV/s.

2. R_{sd} under various V_g sweeping modes.

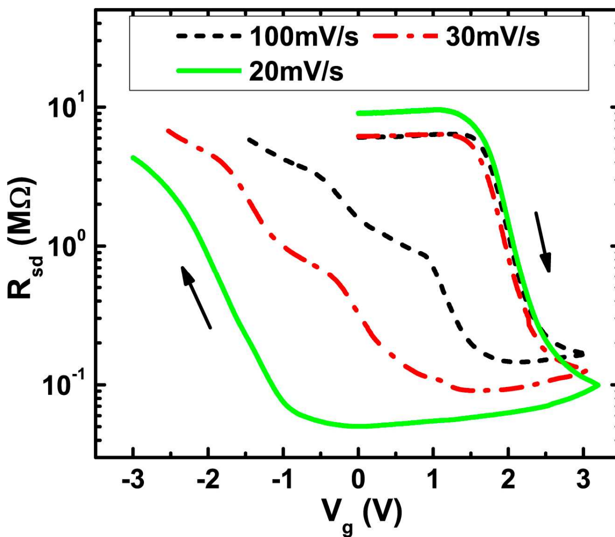

Figure S2. R_{sd}-V_g curves at different V_g sweeping rates. The hysteresis increases with reduced sweeping rate.

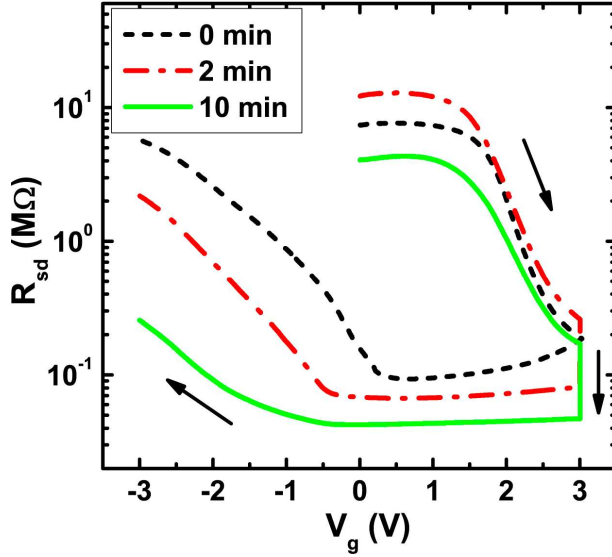

Figure S3. R_{sd}-V_g curves with different waiting times at V_g =3 V before sweeping back. R_{sd} keeps decreasing when V_g is being held at 3V for the waiting time. The hysteresis also increases with increasing waiting time.

3. Discussion of hysteresis and memory behavior.

The $R_{sd} \sim V_g$ dependence exhibits a clear hysteretic and memory behaviour. As shown in Fig. 1**d** and Fig. S2-S3, at the turning point of V_g = 3V, the slope of the $R_{sd}(V_g)$ curve exhibits a memory effect; namely, even though V_g starts to be scanned back away from 3 V, R_{sd} initially continues to decrease following the trend when V_g was scanned forward toward 3 V. This is also consistent with the HfO_2 gating of VO_2 [1], which suggested that VO_2 nanobeam-based field effect transistor devices may be used as non-volatile memories.

The increasing hysteresis width with slower sweeping rate is opposite to kinetic behaviour observed and expected from the low mobility of ions [2]. During the gated surface metal-insulator transition (SMIT), the surface M layer is pseudomorphically clamped to the I-phase VO_2 body. The M phase has a different crystal structure and lattice constant from the I phase [3]. The SMIT thus requires a mechanical relaxation inside the surface layer to accommodate the structural

mismatch, which may be responsible for the wide hysteresis. Near room temperature, slow mechanical relaxation has been widely observed in nanomaterials arising from structural mismatch such as dislocation and domain boundary creep [4]. For example, recently using *in situ* mechanical testing in a transmission electron microscope, we showed wide hysteresis and time delay in the phase transition of a VO_2 nanobeam arising from pinning and depinning, by defects, of domain walls separating different phases [5]. In addition, charge trapping and de-trapping are also a possible origin for the abnormal hysteresis, as been demonstrated in carbon nanotubes transistors in aqueous environments [6]. The exact mechanism of the hysteretic behaviour needs further exploration.

4. I_{sd} vs. V_{sd} at different values of V_g

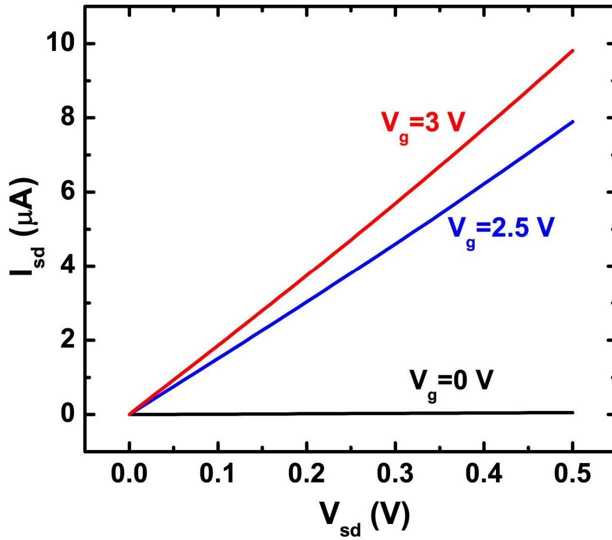

Figure S4. I_{sd}-V_{sd} curves at different values of V_g.

5. Numerical modeling of electrostatic field induced charge accumulation in VO_2.

From the length (10μm), width (500 ~ 1000 nm) and height (~500nm), and resistance (1~5 MΩ) of the un-gated VO_2 nanobeams at the experimental temperature (318K), it is estimated that their I-phase conductivity is 0.1 ~ 0.2/Ωcm. Assuming an electron mobility of 0.1~ 0.5 cm^2/Vs [7, 8],

the carrier density (n) due to background doping (N_d) in the I-phase is estimated to be 10^{18} ~10^{19} /cm^3. This is consistent with typical N_d values reported in VO_2 bulk [8, 9] or thin films [7].

Two-dimensional device simulations were performed using the standard software TCAD SENTAURUS. The dynamic non-local path band-to-band model was used. Standard Shockley-Read-Hall (SRH) recombination and drift-diffusion models were used for carrier transport, and the Fermi statistics was assumed for free charge carriers. For the n$^+$-doped source/drain, an electrically active VO_2 layer of 10^{20} cm^{-3} was assumed to model the Ohmic contacts, the background doping N_d varies from 10^{18} to 10^{19} cm^{-3} for the n channel body, and an equivalent oxide thickness of 0.4 nm was used.

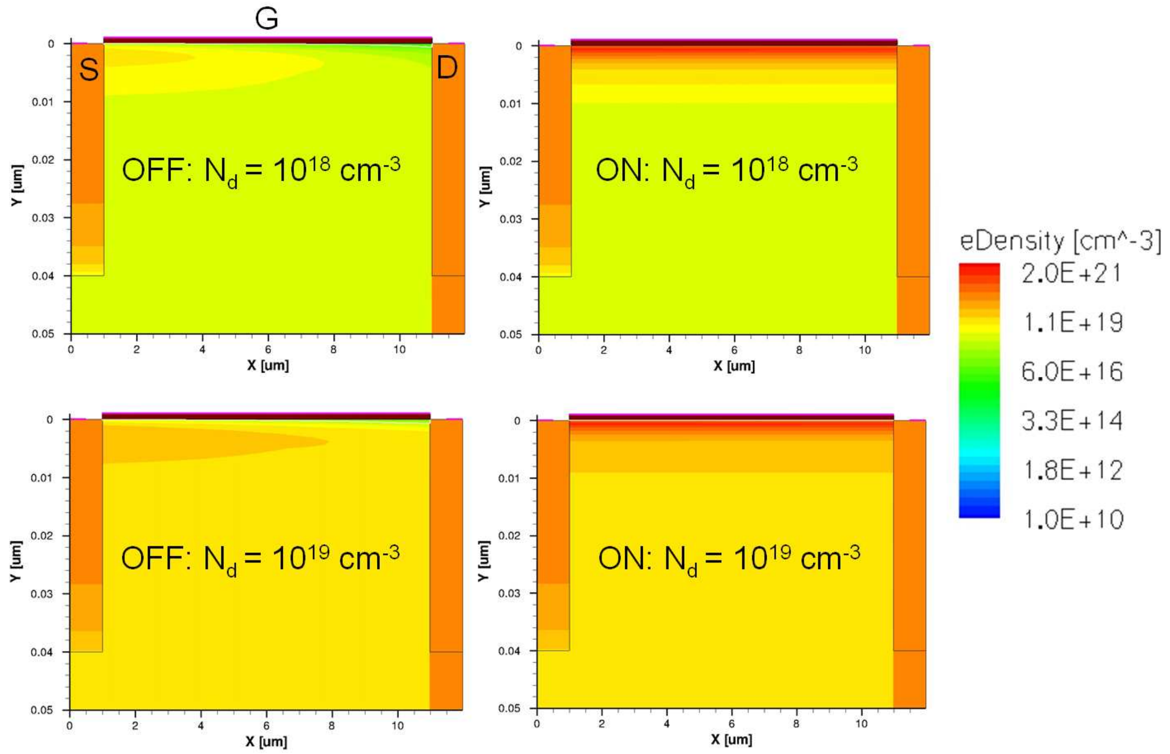

Figure S5. Modeled electron density distribution assuming mere electrostatic charge accumulation *without* the SMIT. The gate-field induced electron accumulation occurs only near the surface within a few nm, leaving the total channel resistance R_{sd} dominated by the bulk. Here the vertical thickness of the channel is 500 nm, but only the top 50 nm is shown for clarity. N_d is the background doping. V_{sd} is 0.2 V and V_g is 0 (OFF) or 3 V (ON).

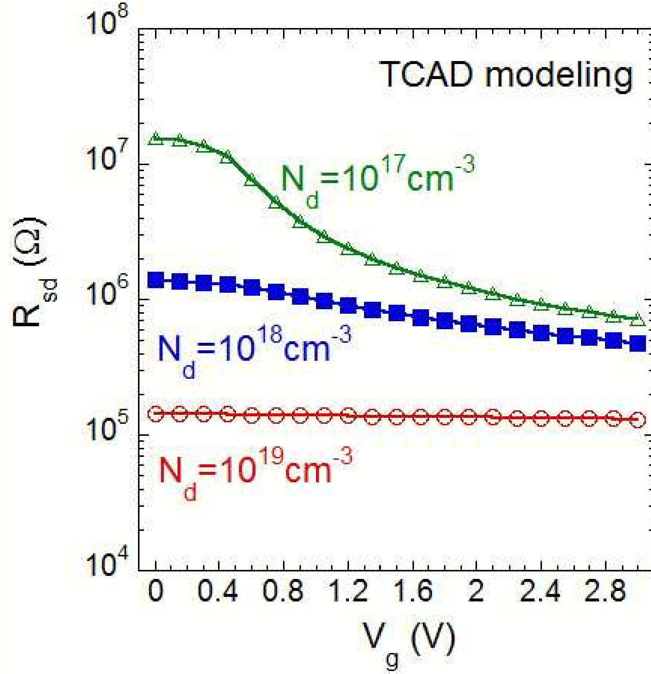

Figure S6. Modeled $R_{sd} \sim V_g$ curves at different background doping N_d, assuming *no* SMIT. Here a VO_2 channel thickness of 500 nm was used. R_{sd} changes by a factor of 3 for $N_d = 10^{18}$ cm^{-3} and remains unchanged for $N_d = 10^{19}$ cm^{-3}. It is clear that an ON/OFF ratio of ~ 100 cannot be explained by this pure electrostatic charge accumulation effect for the VO_2 samples studied that have N_d between 10^{18} and 10^{19} cm^{-3} and thickness of ~ 500 nm.

6. Raman spectra of electrolyte at various gate voltages

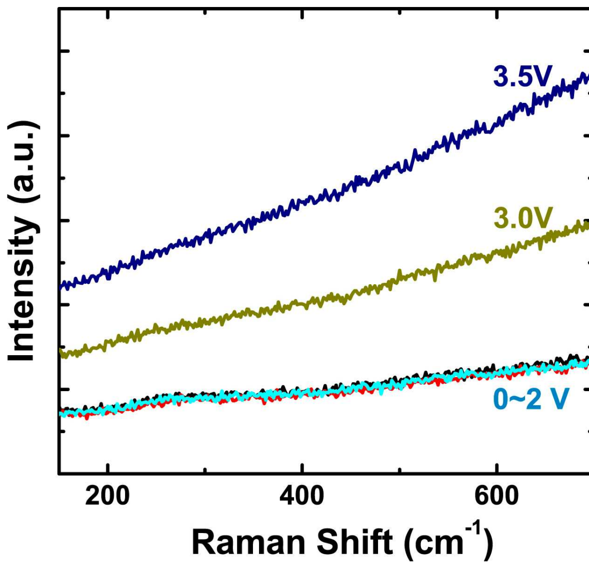

Figure S7. Raman spectra of the Au/Cr electrode immersed in the electrolyte at various gate voltages. This shows that the electrolyte under gating can contribute an increasing strong background in Raman spectroscopy. After subtracting this background, the VO_2 Raman peaks in Fig.2a shows no gate dependence.

7. Gating by using a different ionic liquid (DEME-TFSI)

Another type of common ionic liquid, DEME-TFSI (from Kanto Corp.), was also used as the gating electrolyte to perform the same gating experiments. Before the measurement, the ionic liquid was carefully dried in vacuum (~10^{-5} Torr) at 110 °C for 15 hours, and the devices we used were also dried (but not in touch with the electrolyte) under the same condition; this process aggressively dehydrates the ionic liquid and the devices. As shown in Fig. S8, we compare the gating results before and after the drying processes. As can be seen, for both cases, we observed similar gate modulation of the channel resistance of the same device, while the leakage current through the electrolyte is negeligible (see insets). Note that the ON/OFF ratio for this device is around one order of magnitude, which is smaller than that shown in Fig. 1(d) for a different device. This is because the thickness of the VO_2 nanobeam used here is much thicker (~1.5 μm). The thickness-dependent ON/OFF ratio is also another evidence that the MIT occurs only on the surface. Note that we applied different V_{sd} when sweeping the V_g, therefore the I_{sd} as shown in the insets is different for these two cases.

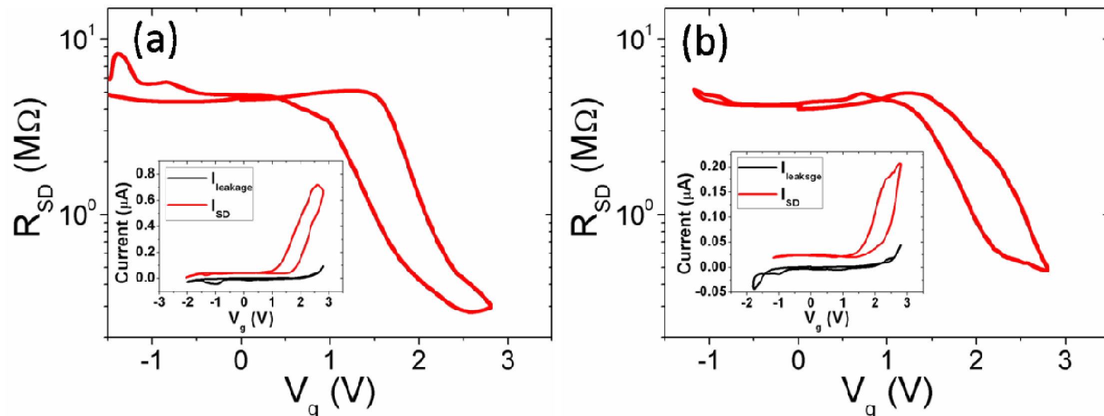

Figure S8. Source-drain resistance as a function of gate voltage on a DEME-TFSI gated device. (a) Pristine device and pristine DEME-TFSI were used. (b) The same device as used in (a), while

both the device and DEME-TFSI were dehydrated by baking the device in vacuum at 110 °C for 15 h prior to electrical measurements. The scanning rate is 20 mV/s. The device has a rectangular cross section, with a thickness of ~ 1.5 μm. The insets show that the leakage current through electrolyte is negligible as compared with the source-drain current during the gating experiment.

8. Details of energy calculation.

(1) Electric field energy in VO_2 and the electric double (Helmholtz) layers

In the Scenario A, the Debye-Hückel approximation was used to calculate the carrier distribution along the depth of surface, $n(z)$, with a screening length given by

$$\lambda_{DH} = \sqrt{\frac{\varepsilon_{VO2}^{I} k_B T}{e^2 n_{th}}},$$

where $\varepsilon_{VO2}^{I} = 24\,\varepsilon_0$ is the dielectric constant of VO_2 in the I phase, n_{th} is the threshold of carrier density triggering the MIT. Under this approximation, the electrical potential $\varphi(z)$, the electric field $F(z)$, and the net carrier density $n(z) - n_b$ inside VO_2 can all be approximately expressed in the form of $\sim \exp(z/\lambda_{DH})$. Here n_b ~ 10^{18} cm^{-3} is the background carrier density of VO_2, z varies from $-\infty$ to 0, and $z = 0$ is the VO_2 surface. The coefficient of this exponential dependence for $\varphi(z)$, $F(z)$, and $n(z) - n_b$ are related to the boundary condition of $\varphi(z = 0) = \varphi_0$ and the Gauss' law. The depth within which the carrier density exceeds the threshold n_{th} is given by

$$z_{th} = \lambda_{DH} \ln \frac{\varepsilon_{VO2}^{I} \varphi_0}{(n_{th} - n_b) \cdot e \cdot \lambda_{DH}^2}.$$

The surface potential φ_0 is linked to V_g by the continuity condition of electric displacement at the surface of VO_2. By assuming the same potential drop across both Helmholtz layers at the electrolyte / VO_2 and the electrolyte / gate electrode interfaces, one has

$$\varphi_0 \approx \frac{V_g}{1+\dfrac{\varepsilon_{VO2}^{I}\cdot 2d_{HL}}{\varepsilon_{electrolyte}\cdot \lambda_{DH}}},$$

where $\varepsilon_{electrolyte} = 10\varepsilon_0$ is dielectric constant of the electrolyte, and d_{HL} ~ 1 nm is the thickness of the Helmholtz layer. In Scenario A, the electric field energy in the VO_2 and the Helmholtz layers can be obtained,

$$E_{VO2}^{A} \approx \int_{-z_{th}}^{0} \frac{1}{2}\varepsilon_{VO2}^{I}\left[F\left(z\right)\right]^2 dz \approx \frac{\varepsilon_{VO2}^{I}\varphi_0^2}{4\lambda_{DH}},$$

$$E_{HL}^{A} \approx 2\times\frac{1}{2}\varepsilon_{electrolyte}F_{HL}^{2}\times d_{HL} = \varepsilon_{electrolyte}\left(V_g-\varphi_0\right)^2 \Big/ 4d_{HL}.$$

In Scenario B, the SMIT occurs within the thickness $d_{SMIT} = z_{th}$. The layer turns into M phase while the rest of the VO_2 body is in the I phase with depletion of electrons near interface, forming a Schottky barrier inside VO_2. The contact potential (Fermi energy difference) between the M and the I phases is assumed to be ~ 0.3 eV, half of the bandgap of VO_2 [3]. In the M layer, the Thomas-Fermi approximation is applied with a screening length $\lambda_{TF}^{B} = \sqrt{\frac{\varepsilon_{VO2}^{M}\pi^2\hbar^2}{m_M^* e^2\left(3\pi^2 n\right)^{3/2}}}$, where $\varepsilon_{VO2}^{M} \approx 9\,\varepsilon_0$, $m_M^* \approx 5m_0$, and n ~ 10^{22} cm^{-3}. In the I part underneath, the Debye-Hückel Approximation was used to estimate the screening length $\lambda_{DH}^{B} = \sqrt{\frac{\varepsilon_{VO2}^{I}k_B T}{e^2 n_b}}$. Similar to the Scenario A, the electric field in the VO_2 and the Helmholtz layers was determined, and the energies were calculated.

(2) Gibbs free energy difference $\Delta G = G_I - G_M$.

When the carrier density n exceeds the threshold n_{th}, G_M becomes lower than G_I. Their

difference $\Delta G = G_I - G_M$ as a function of n can be estimated in the following way. According to the Landau theory, G_M and G_I are expanded at the MIT point as a function of $\ln n$,

$$G_I(\ln n) = G_I^0 + \ln\frac{n}{n_{th}} \cdot \left.\frac{\partial G_I}{\partial \ln n}\right|_{n=n_{th}} + \cdots$$

$$G_M(\ln n) = G_M^0 + \ln\frac{n}{n_{th}} \cdot \left.\frac{\partial G_M}{\partial \ln n}\right|_{n=n_{th}} + \cdots$$

VO_2 undergoes a first-order MIT, so $G_I^0 = G_M^0$, and thus,

$$\Delta G = G_I(n) - G_M(n) \approx \ln\frac{n}{n_{th}} \cdot \left.\frac{\partial \Delta G}{\partial \ln n}\right|_{n=n_{th}} = \ln\frac{n}{n_{th}} \left.\frac{\partial \Delta G}{\partial T} \middle/ \frac{\partial \ln n}{\partial T}\right|_{n=n_{th}}$$

Because $\left.\frac{\partial \Delta G}{\partial T}\right|_{n=n_{th}} = \Delta S|_{n=n_{th}} = \frac{\Delta H}{T_{th}} = \frac{L}{T_{th}}$, where ΔS is the change of entropy, ΔH is the change of enthalpy, L is the latent heat of the MIT of VO_2, and T_{th} is the temperature of the phase transition. Here we use the parameters of I-phase VO_2 for an estimation of the free energy difference because many parameters of the metal phase are unknown. Considering thermal activation of free electron density, $n \propto \exp(-E_a/k_B T)$, where E_a is the activation energy in I-phase VO_2, so $\left.\frac{\partial \ln n}{\partial T}\right|_{n=n_{th}} = \frac{E_a}{k_B T_{th}{}^2}$. As a result,

$$\Delta G(n) \approx \ln(n/n_{th}) \cdot (L \cdot k_B T / E_a).$$

The overall change in ΔG was obtained by integrating $\Delta G(n)$ over the depth d_{SMIT} using the solved $n(z)$ at different V_g,

$$\Delta G \approx \frac{L \cdot k_B T \cdot d_{SMIT}}{E_a}\left(\frac{d_{SMIT}}{2\lambda_{DH}} - \ln\frac{n_{th}}{n_{th} - n_b}\right).$$

References for supporting information

1. Sengupta, S.; Wang, K.; Liu, K.; Bhat, A. K.; Dhara, S.; Wu, J.; Deshmukh, M. M. *Appl. Phys. Lett.* **2011**, *99*, 062114.
2. Khanal, D. R.; Walukiewicz, W.; Grandal, J.; Calleja, E.; Wu, J. *Appl. Phys. Lett.* **2009**, *95*, 173114 /1-3.
3. Eyert, V. *Ann. Phys.-Berlin* **2002**, *11*, 650-702.
4. Meyers, M. A.; Mishra, A.; Benson, D. J. *Prog. Mater. Sci.* **2006**, *51*, 427-556.
5. Guo, H.; Chen, K.; Oh, Y.; Wang, K.; Dejoie, C.; Asif, S. A. S.; Warren, O. L.; Shan, Z. W.; Wu, J.; Minor, A. M. *Nano Lett.* **2011**, 11, 3207-3213.
6. Kim, W.; Javey, A.; Vermesh, O.; Wang, Q.; Li, Y.; Dai, H. *Nano Lett.* **2003**, *3*, 193-198.
7. Ruzmetov, D.; Heiman, D.; Claflin, B. B.; Narayanamurti, V.; Ramanathan, S. *Phys. Rev. B* **2009**, *79*, 153107.
8. VO_2: resistivity, conductivity, photoconductivity. In Springer Materials - The Landolt-Börnstein Database(eds. Madelung, O., Roessler, U. & Schulz, M.).
9. Berglund, C. N.; Guggenheim, H. J. *Phys. Rev.* **1969**, *185*, 1022-1033.